Time- frequency representation of earthquake accelerograms and inelastic structural response records using the adaptive chirplet decomposition and empirical mode decomposition

Authors

P.D. Spanos[1,*] A. Giaralis[2], N.P. Politis[3]

Affiliations

[1]L. B. Ryon Chair in Engineering, Rice University, Houston, Texas

[2]Ph.D. Candidate, Department of Civil Engineering, Rice University, Houston, Texas

[3]Floating Systems Engineer, BP America Inc.

Abstract

In this paper the adaptive chirplet decomposition combined with the Wigner-Ville transform and the empirical mode decomposition combined with the Hilbert transform are employed to process various nonstationary signals (strong ground motions and structural responses). The efficacy of these two adaptive techniques for capturing the temporal evolution of the frequency content of specific seismic signals is assessed. In this respect, two near- field and two far- field seismic accelerograms are analyzed. Further, a similar analysis is performed for records pertaining to the response of a 20-story steel frame benchmark building excited by one of the four accelerograms scaled by appropriate factors to simulate undamaged and severely damaged conditions for the structure. It is shown that the derived joint time- frequency representations of the response time

[*] Pol D. Spanos, George R. Brown School of Engineering, L. B. Ryon Chair in Engineering, Rice University, MS 321, P.O. Box 1892, Houston, TX 77251, U.S.A.

e-mail: spanos@rice.edu

histories capture quite effectively the influence of nonlinearity on the variation of the effective natural frequencies of a structural system during the evolution of a seismic event; in this context, tracing the mean instantaneous frequency of records of critical structural responses is adopted.

The study suggests, overall, that the aforementioned techniques are quite viable tools for detecting and monitoring damage to constructed facilities exposed to seismic excitations.

Keywords: time-frequency representation; chirplets; empirical mode decomposition; intrinsic modes; accelerograms; nonlinear structural response; damage detection

1. Introduction

Transient signals encountered in earthquake engineering and structural dynamics are inherently nonstationary in the sense that both their frequency content and amplitude vary with time. Typical earthquake accelerograms exhibit a time-evolving frequency composition due to the dispersion of the propagating seismic waves, and a time-decaying intensity after a short initial period of development. Structural systems are characterized by their natural frequencies and modes of vibration, rendering their response to strong ground motions a relative resonance phenomenon. Thus, capturing the time-varying dominant frequencies present in a seismic accelerogram facilitates the assessment of its structural damage potential. Furthermore, the time histories tracing certain structural response quantities, such as floor displacements and inter-story drifts of a building under seismic excitation, are also amenable to treatment as nonstationary signals. Their

evolving frequency content provides valuable information about the possible level of global structural damage caused by the ground motion. Signals of this kind require a joint time- frequency analysis.

Ordinary Fourier analysis has been used for several decades in earthquake engineering for representing the frequency content of seismic events. In this regard there are obvious limitations, since the Fourier transform can only provide an "average" spectral decomposition of a signal. The availability of more powerful computers, advances in applied mathematics [1-8], and the development of fast algorithms [7-12] have facilitated the application of time-frequency analysis techniques in various engineering fields over the past years. These techniques can be loosely divided into adaptive and non-adaptive. It is the intention of this paper to exploit certain adaptive methods for capturing the temporal variation of the frequency content of earthquake accelerograms and of seismic structural response signals. However, it is emphasized that techniques belonging to both the above categories constitute viable tools for the purpose.

To ensure completeness and to enhance the readability of the manuscript a conspectus of the commonly used non-adaptive methods is first provided before focusing on the adaptive methods that the present study considers.

Introduced by Gabor [13], the first and most widely used method for joint time-frequency representation of non-stationary signals utilizes the so-called *short-time Fourier transform* (STFT) to project a signal onto a family of appropriately shifted (translated in time domain), and modulated (translated in frequency domain), copies of a constant width window function. Then the *spectrogram* defined by the modulus of the STFT squared can be interpreted as a distribution of the signal energy on the time-

frequency plane. This gives rise to a non- adaptive analysis procedure with significant time- frequency resolution limitations; once the window function is chosen, the frequency and time resolutions are fixed for all frequency bands and all times [1,7].

A more flexible representation of a signal with non-constant windowing can be achieved by the *wavelet transform* (WT) [2,3], which incorporates a family of oscillatory functions generated by appropriately shifting and scaling a single "mother wavelet" function of certain frequency content and of localized energy in time. The flexibility of the WT stems from the scaling operation and the wave-like form of the mother wavelet: dilating and contracting the support of a wavelet (scaling) allows the adjustment of its time duration, while narrows and expands the bandwidth, respectively. The *scalogram* defined in a similar way from the WT as the spectrogram from STFT yields enhanced time resolution representations for short-lived high-frequency phenomena, and frequency resolution for long-lasting low-frequency phenomena.

Obviously, the WT is a potent tool for analyzing and representing nonstationary signals in the time-frequency domain. In a recent review article by Spanos and Failla [14] an extensive reference list is provided citing numerous publications incorporating the wavelet analysis for various structural engineering and vibration applications.

Alternatively, adaptive signal processing techniques can be adopted for effectively capturing local variations of a much wider variety of signals and for the efficient representation of signals by much fewer terms than the classic non-adaptive methods. In this context, the *matching pursuit* (MP) algorithm [9-11] for the decomposition of the signal on a *Gaussian chirplet* set of functions (Gaussian chirplet dictionary), and the *empirical mode decomposition* (EMD) which provides a case-

specific data-driven decomposition of a signal into non predefined functions [6] are exclusively used in the present work.

Chirplets can be construed as generalized wavelets, containing more "degrees of freedom" than a wavelet since a chirplet waveform can be induced to "shear" and "rotation" in the time-frequency plane, apart from translation and scaling [4,5]. In this case, the adaptive character of the method stems from the fact that a Gaussian chirplet set of functions is redundant (over-determined); not all functions of the set are necessary for the representation of a particular signal and thus different subsets of chirplets is chosen for the representation of different signals. The MP algorithm seeks the optimal unfolding of any signal in the time-frequency plane. More importantly, the Wigner-Ville distribution (WVD) of a signal decomposed by Gaussian chirplet functions [5] posses all the attractive mathematical properties of the WVD [1] and yields a non-negative and cross-term free bilinear distribution on the time-frequency plane of exceptional resolution [7]. Further, the WVD lends itself to mathematical manipulations that lead to important concepts like the *mean instantaneous frequency* (MIF) [7,14].

As far as the EMD is concerned, it decomposes any signal into several *monocomponent* signals [1] extracted from the initial signal itself in the form of *intrinsic mode functions* (IMFs) [5], for which the *instantaneous frequency* (IF) [1,15] has physical meaning. Then, the MIF and the Hilbert spectrum of all IMFs can be computed to reach an alternative time-frequency representation of the initial multicomponent signal. The algorithm for the EMD is simple, iterative, and computationally demanding in the case of long duration signals. Flandrin et al. [16] have used EMD in stochastic analysis to show that it exhibits several properties which are common with the WT, as self-

similarity, quasi-decorrelation, and variance progression. However, there is no theoretical definition of the decomposition in terms of analytic expressions for the IMFs which depend on the settings of the EMD algorithm.

Wang et al. [17] considered the analysis of recorded earthquake accelerograms via the adaptive chirplet decomposition to define a physically meaningful time and frequency dependent envelop function in the context of defining appropriately an evolutionary power spectrum. Hilbert spectra representations using IMFs have been used to capture the spectral characteristics of earthquake accelerograms [18-21], in structural damage detection [22-24], and in soil dynamics problems [25]. Many researchers have compared the results of the EMD versus the traditional Fourier analysis and/or non-adaptive methods for time-frequency representation such as the WT in the light of the aforementioned and other applications in engineering [18,22,23,25-27].

Since the EMD is a purely numerical semi-empirical method it seems more appropriate to evaluate its effectiveness for joint time-frequency representation of signals by comparison with numerical results obtained from other adaptive methods, like the adaptive chirplet decomposition. Herein, a detailed study of strong ground motions is conducted by means of the adaptive chirplet decomposition and the EMD, to explore their time-frequency representation capabilities, investigate their needed level of sophistication, assess their comparative efficiency and extract information related to the MIF as computed by both techniques. In this regard, joint time- frequency representations are provided in the form of the WVD and Hilbert spectra respectively for two near- field, and two far- field recorded seismic data [28,29], together with time-histories of the MIF. Furthermore, the same adaptive methods are used to extend early works such as that of

Roesset [30], to capture the influence of nonlinearity on the variation of the effective natural frequencies of a structural system during the evolution of a seismic event. For this purpose nonlinear, step-by-step in time, analysis is performed for a benchmark 20- story steel frame [28,29], excited by one of the above mentioned strong ground motions scaled by various factors. Appropriate numerical results for certain structural response time histories processed by the previously mentioned adaptive methods are given for undamaged and severely damaged conditions, showing that the MIF can be considered as a promising global structural damage detection tool.

2. Mean instantaneous frequency via the adaptive chirplet decomposition

In this section, closed formulas for the mean instantaneous frequency (MIF) and for the adaptive periodogram (AP) are derived by application of the Wigner- Ville distribution (WVD) on the decomposed signal. For the signal decomposition, Gaussian chirplets and the Matching Pursue (MP) algorithm are utilized.

2.1 Signal decomposition: The Matching Pursue algorithm

Consider the *Gaussian function*

$$g(t) = \sqrt[4]{\frac{1}{\pi}} e^{\left\{-\frac{1}{2}t^2\right\}} \tag{1}$$

The *Gaussian chirplet* $h_k(t)$ is a four- parametered function described by the equation

$$h_k(t) = \sqrt[4]{\frac{a_k}{\pi}} e^{\left\{-\frac{a_k}{2}(t-t_k)^2\right\}} e^{i\left\{\frac{\beta_k}{2}(t-t_k)^2\right\}} e^{i\{\omega_k(t-t_k)\}} \tag{2}$$

This function involves scaling by the parameter α_k, shifting in time and in frequency by t_k and ω_k, respectively, and linear frequency modulation by chirprate β_k [4]. Note that Eq. (2) is deliberately given in a non-compact form, for better visualization of the four

successive transformations imposed on the Gaussian function. If there is no frequency modulation, that is $\beta_k = 0$, the Gaussian chirplet becomes a *Gabor atom*.

Consider a signal $x(t)$ of finite *energy in the time domain* $|x(t)|^2$ satisfying the condition

$$E = \int_{-\infty}^{\infty} |x(t)|^2 \, dt < \infty , \tag{3}$$

where E is the total energy of the signal.

Traditional Fourier analysis utilizes the *Fourier Transform (FT),* defined by

$$X(\omega) = \int_{-\infty}^{\infty} x(t) e^{-i\omega t} dt , \tag{4}$$

to project the signal $x(t)$ onto the basis of the trigonometric (sinusoid) functions $\{e^{i\omega t}\}_{\omega \in R}$. By Parseval's theorem, the FT preserves the signal energy, and thus the modulus of the FT squared $|X(\omega)|^2$, commonly called as the *energy density spectrum*, can be viewed as a distribution of the energy of $x(t)$ in the frequency domain [1]. Sinusoids correspond to delta functions in the frequency domain, yielding the best possible spectral resolution. However, they possess no localization capabilities in the time domain, being functions of infinite support. Thus, the energy density spectrum depicts the overall frequency content of a signal with the highest possible resolution, but provides no information about the time that each frequency component was present in the signal.

Developed independently by Mallat and Zhang [9], and Qian and Chen [10], the matching pursue (MP) algorithm, allows the decomposition of any signal satisfying Eq.

(3) into a linear combination of any set of analyzing functions (dictionary) [8]. Note that Gaussian chirplets attain finite effective support both in the time and in frequency domain. They are capable of capturing the local characteristics of a signal in both domains and, thus, are suited for the decomposition of highly nonstationary signals.

Employing a set (dictionary) comprising Gaussian chirplets, the MP yields the following decomposition of the signal $x(t)$:

$$x(t) = \sum_k A_k h_k(t) \tag{5}$$

The expansion coefficients A_k are determined sequentially via successive approximations of the signal by orthogonal projections (inner products), on the elements of the dictionary. This is equivalent to the solution of the optimization problem

$$|A_k|^2 = \max_{h_k} |\langle x_k(t), h_k(t) \rangle|^2 = \max_{h_k} \left| \int_{-\infty}^{\infty} x_k(t) h_k(t)\, dt \right|^2 \tag{6}$$

First, the original signal $x(t) = x_k(t)$ for k = 0 is projected on all the functions of the dictionary and the coefficient A_0 is determined from Eq. (6). Then, the residual $x_{k+1}(t)$ is determined

$$x_{k+1}(t) = x_k(t) - A_k h_k(t) \tag{7}$$

This procedure, described above for the original signal, is repeated for the residual iteratively, and the algorithm terminates when the energy of the residual reaches a desired predefined level that obviously characterizes the quality of the approximation.

Note that the MP algorithm imposes no restrictions on the analyzing functions. Consider next unit energy functions as those of Eq. (2). That is require that

$$\left\| h_k(t) \right\|^2 = \int_{-\infty}^{\infty} \left| h_k(t) \right|^2 dt = 1 \tag{8}$$

Then it can be readily proved that the energy of the signal can be expressed as [14]

$$\left\| x(t) \right\|^2 = \sum_{k=0}^{\infty} |A_k|^2 \tag{9}$$

showing that the previously described decomposition preserves the signal energy.

The algorithm that was outlined by Eqs. (5)-(7) is based on a predetermined dictionary, whose size influences the accuracy of the signal representation. More accurate representations require larger dictionaries, and thus excessive computations. The efficient and accurate numerical implementation of the MP algorithm is an open research area. In the present study a refinement scheme introduced by Yin et al. [11], is adopted, which allows the use of a coarse chirplet dictionary for a first estimate, and then refinement of the analysis by a curve fitting process.

2.2 Wigner-Ville distribution of the decomposed signal

Upon expressing the signal $x(t)$ as a weighted sum of chirplet functions, a suitable representation on the time-frequency plane must be established. In the present work the bilinear Wigner-Ville distribution (WVD), is chosen. The WVD of a signal $x(t)$ is defined by the equation [1]

$$WVD_x(t,\omega) = \frac{1}{2\pi} \int_{-\infty}^{\infty} x\left(t + \frac{1}{2}\tau\right) x^*\left(t - \frac{1}{2}\tau\right) e^{-i\omega\tau} d\tau \,, \tag{10}$$

and has finite support both in the time and frequency domains. In terms of the STFT, the signal is analyzed in this case by using a modulated and appropriately shifted window which coincides with the signal itself after being time-reversed at each time instant t. Although this interpretation is neither mathematically helpful nor what inspired the

inventors of the WVD, it does provide an intuitive perspective on the formulation of the distribution, and reveals its self-adaptive character.

For any finite energy signal $x(t)$ the WVD satisfies always the so-called marginal distributions of the signal [1]. That is,

$$\frac{1}{2\pi}\int_{-\infty}^{\infty} WVD_x(t,\omega)\,d\omega = |x(t)|^2 \quad and \quad \int_{-\infty}^{\infty} WVD_x(t,\omega)\,dt = |X(\omega)|^2 . \tag{11}$$

From Eq. (11) it is deduced that the WVD preserves the energy of the signal.

Further, $x(t)$ can be expressed in the polar form

$$x(t) = \mathrm{Re}\left[C(t)e^{i\varphi(t)}\right], \tag{12}$$

where $C(t)$ and $\varphi(t)$ are the magnitude and phase, respectively. Then the first order conditional moment of time is expressed by the equation

$$\langle\omega\rangle_t = \frac{\frac{1}{2\pi}\int_{-\infty}^{\infty}\omega WVD_x(t,\omega)\,d\omega}{\frac{1}{2\pi}\int_{-\infty}^{\infty} WVD_x(t,\omega)\,d\omega} = \frac{1}{2\pi|x(t)|^2}\int_{-\infty}^{\infty}\omega WVD_x(t,\omega)\,d\omega = \dot{\varphi}(t), \tag{13}$$

and defines the mean instantaneous frequency (MIF) of $x(t)$, if $x(t)$ is a multicomponent signal; and the instantaneous frequency (IF) of $x(t)$, if $x(t)$ is a monocomponent signal [1,7,15]. In Eq. (13) and hereafter the dot over a symbol denotes differentiation with respect to time.

The concept of the IF is interwoven with the study of non-stationary signals; it serves as a tool to quantify the frequencies present in a signal at each time instant t. The definition of the optimal mathematical measure of the temporal change of the frequency content of a signal is still an open issue for the case of multicomponent signals, even

though it is an intuitive concept. However, in the case of monocomponent signals, the IF as defined in Eq. (13) is considered quite appropriate.

Besides the aforementioned attractive mathematical properties, the WVD exhibits two general drawbacks.

The first drawback is that it often attains negative values in certain regions of the time-frequency plane [1] rendering the physical interpretation problematic. This feature is inherent in every bilinear distribution satisfying the marginal distributions, as expressed by Eq. (11). Note however, that the Gaussian chirplet defined by Eq. (2) has the WVD

$$WVD_{h_k}(t,\omega) = 2\, e^{\left\{-a_k (t-t_k)^2\right\}} e^{i\left\{-\frac{1}{a_k}\left[(\omega-\omega_k)-\beta_k (t-t_k)\right]^2\right\}}, \tag{14}$$

which is non-negative everywhere; in this case the WVD leads to a valid time-frequency density function of the signal.

The second main drawback of the WVD that in general limits its use in favor of the spectrogram, is the so-called cross-term interference [1,7]. It is caused by the fact that the WVD is non-additive. Indeed, application of the WVD in both sides of Eq. (5) yields

$$WVD_x(t,\omega) = \sum_k |A_k|^2 WVD_{h_k}(t,\omega) + \sum_{k\neq q} A_k A_q WVD_{h_k h_q}(t,\omega), \tag{15}$$

where the first summation corresponds to the auto-WVD terms of the analyzing chirplet functions, and the second summation corresponds to their cross-WVD terms. In many practical cases, the latter terms, inherent in all multicomponent signals, corrupt the time-frequency representation severely and induce poor resolution in the WVD. It is clear that the extent of the cross-term interference depend on the decomposition of the signal. It can be readily shown using the energy preservation properties of the MP and of the WVD that the energy of the cross-WVD terms in the above equation is zero [7]. That is,

$$\sum_{k\neq q} A_k A_q WVD_{h_k h_q}(t,\omega) = 0\,. \tag{16}$$

Thus, the cross-term free *adaptive spectrogram* (AS) of the decomposed signal $x(t)$ using the MP is defined as [10]

$$AS_x(t,\omega) = \sum_k |A_k|^2 WVD_{h_k}(t,\omega) = 2\sum_k |A_k|^2 e^{\left\{-a_k(t-t_k)^2\right\}} e^{\left\{-\frac{1}{a_k}\left[(\omega-\omega_k)-\beta_k(t-t_k)\right]^2\right\}} \tag{17}$$

Obviously, AS is always positive and preserves the energy of the original signal. Clearly, it serves as a quite effective tool of representing any signal in the joint time-frequency domain incorporating all the advantages of the WVD and none of its drawbacks.

2.3 Mean instantaneous frequency and adaptive periodogram

The *adaptive periodogram* (AP) of the analyzed signal $x(t)$ can be obtained in a closed form using Eqs. (11) and (17). That is,

$$AP_x(\omega) = \int_{-\infty}^{\infty} AS_x(t,\omega)\,dt = 2\sum_k |A_k|^2 \sqrt{\frac{\pi}{\gamma_k}} e^{\left\{-\frac{(\omega-\omega_k)^2}{\gamma_k}\right\}};\ \gamma_k = \frac{a_k^2+\beta_k^2}{a_k}\,. \tag{18}$$

The MIF can be obtained as the conditional average of the WVD for a particular time t by combining Eqs. (11), (13) and (15). Specifically, after some algebraic manipulation one finds that

$$\langle\omega\rangle_t = \frac{\frac{1}{2\pi}\int_{-\infty}^{\infty} \omega WVD_x(t,\omega)\,d\omega}{\frac{1}{2\pi}\int_{-\infty}^{\infty} WVD_x(t,\omega)\,d\omega} = \frac{2\sum_k |A_k|^2 \sqrt{a_k\pi}\left(\omega_k+\beta_k(t-t_k)\right)e^{\left\{-a_k(t-t_k)^2\right\}}}{\sum_k |A_k|^2 \sqrt{a_k\pi}\, e^{\left\{-a_k(t-t_k)^2\right\}}} = MIF\,. \tag{19}$$

The analytical expressions derived herein for the AP (Eq. (18)), and the MIF (Eq. (19)) allow for their robust computation independently of the AS. In this manner, if these are

indeed the only quantities of interest, the computationally-demanding determination of the AS can be circumvented.

3. Hilbert spectrum and mean instantaneous frequency via the Empirical Mode Decomposition

The Empirical Mode Decomposition (EMD) is a numerical data-driven algorithmic procedure for the decomposition of nonstationary signals into a finite number of non predefined case-specific functions, the Intrinsic Mode functions (IMFs) [6]. An IMF is defined in Huang et al [6] as a function which satisfies the following two conditions: (a) the number of the zero crossings and the number of extrema must be either equal or differ by one and (b) the mean value of the local minima envelope and the local maxima envelopes of the function must be zero. Let a signal be heuristically construed as a superposition of "fast" oscillations on top of "slower" oscillations. Then, the EMD identifies locally the fastest oscillating IMF by an iterative "sifting" procedure, subtracts it from the signal, and iterates on the residual [6,12,16]. Assuming that the energy of the final residue is negligible, the EMD yields the following decomposition of a finite energy signal $x(t)$:

$$x(t) = \sum_{j=1}^{N} b_j(t), \tag{20}$$

where $b_j(t)$ is the j^{th} IMF. Associated with each IMF is the *analytic signal* written in polar form as

$$z_j(t) = a_j(t) e^{i\varphi_j(t)}, \tag{21}$$

where $a_j(t) = \sqrt{b_j^2(t) + \tilde{b}_j^2(t)}$ is the magnitude, $\varphi_j(t) = \arctan\dfrac{\tilde{b}_j(t)}{b_j(t)}$ is the phase, and $\tilde{b}_j(t)$ denotes the Hilbert transform of the j[th] IMF [1], given by the equation

$$\tilde{b}_j(t) = \frac{1}{\pi}\int \frac{b_j(s)}{t-s} ds \,. \tag{22}$$

The salient property of the IMFs is that they are monocomponent signals and therefore, the IF of the j[th] IMF at time *t* is appropriately defined as the derivative of the phase of its analytic signal [15]

$$\omega_j(t) = \dot{\varphi}_j(t) = \frac{b_j(t)\dot{\tilde{b}}_j(t) - \dot{b}_j(t)\tilde{b}_j(t)}{b_j^2(t) + \tilde{b}_j^2(t)} \,. \tag{23}$$

By making use of Eqs. (20) and (21) the analytic signal $\hat{x}(t)$ of the original signal $x(t)$ equals the sum of the analytic signals $z_j(t)$ of the IMF components $b_j(t)$. That is

$$\hat{x}(t) = \sum_{j=1}^{N} z_j(t) = \sum_{j=1}^{N} a_j(t) e^{i\int \omega_j(t)dt} \,. \tag{24}$$

Then the *Hilbert spectrum* of $\hat{x}(t)$ defined as

$$H_x(t,\omega) = \sum_{j=1}^{N} a_j\left(t, \omega_j(t)\right) = \sum_{j=1}^{N} a_j(t)\delta\left(\omega - \omega_j(t)\right), \tag{25}$$

constitutes a time-frequency representation of the signal $x(t)$ and is an amalgamation of the individual Hilbert spectra of each of the analytic IMFs.

In this case, it is natural to define the MIF as the weighted average of the IFs $\omega_{i_j}(t)$ of the individual IMFs:

$$\left\langle \omega \right\rangle_t = \frac{\sum_{j=1}^{N} a_j^2(t)\,\omega_j(t)}{\sum_{j=1}^{N} a_j^2(t)} = MIF \tag{26}$$

For discrete signals, a straightforward computation of the IF using Eq. (23) is numerically sensitive since it requires the calculation of two additional derivatives. Moreover, for noisy signals this approach yields IF of high variance which are not readily amenable to physical interpretation. Better results can be obtained by using a numerical differentiation method directly on the phase as given by Eq. (21), after applying a low-pass filter to the analytic signal [31]. In this context, a fourth- order estimation

$$\omega_j[n] = \dot{\varphi}_j[n] = \frac{1}{12}\left(\varphi_j[n-2] - 8\varphi_j[n-1] + 8\varphi_j[n+1] - \varphi_j[n+2]\right) \tag{26}$$

of the IF is adopted in the present study, and at the end-points the five- point formula

$$\omega_j[n] = \dot{\varphi}_j[n] = \pm\frac{1}{12}\left(-25\varphi_j[n] + 48\varphi_j[n\pm1] - 36\varphi_j[n\pm2] + 16\varphi_j[n\pm3] - 3\varphi_j[n\pm4]\right) \tag{27}$$

is used, following Olhede and Walden [32].

It is emphasized that the IMFs are obtained by the application of an empirical algorithmic procedure and, thus, cannot be analytically expressed. Their form depends primarily on the settings and assumptions adopted, that is, intermittency frequency, interpolation method, and stopping criteria, during the sifting operations that the EMD incorporates for the extraction of the IMFs from the signal [26]. Besides the original algorithm introduced by Huang et al. [6], there exist several other approaches in the literature regarding the interpolation procedure and the stopping criteria [12,16,26]. In practice, a trial and error procedure for the fine- tuning of these settings may not be feasible since the EMD is quite demanding in terms of computational power, especially for long data sequences.

Recently, Yan and Miyamoto [23] incorporated entropy concepts to obtain rational case-specific values for the stopping criteria and various thresholds featured in the EMD algorithm, instead of using the default values proposed by Rilling et al [12]. This approach increases further the computational time by an amount that in many cases is disproportional to the additional improvement achieved.

The EMD algorithm and the default stopping criteria proposed in [12], were adopted for all the ensuing numerical analyses. Further numerical experimentation on the EMD would considerably increase the requisite computations to the extent of rendering the two methods incomparable.

4. Historic accelerograms and the benchmark structural system description

Four historic earthquake records are studied to assess the appropriateness of the adaptive chirplet decomposition and the EMD to provide information about the time-frequency characteristics of ground acceleration records pertaining to major earthquake events. The El Centro (N-S component recorded at the Imperial Valley Irrigation District substation in El Centro, California, during the Imperial Valley, California earthquake of May 18, 1940), and the Hachinohe (N-S component recorded at Hachinohe City during the Takochi-oki earthquake of May 16, 1968), earthquakes have been selected as far-field examples. The Northridge (N-S component recorded at Sylmar County Hospital parking lot in Sylmar, California, during the Northridge, California earthquake of January 17, 1994), and the Kobe (N-S component recorded at the Kobe Japanese Meteorological Agency (JMA) station during the Hyogo-ken Nanbu earthquake of January 17, 1995),

earthquakes have been chosen as near-field examples [28,29]. Fig. (1) shows the accelerograms of these strong ground motions.

The potential of the adaptive chirplet decomposition and the HHT for capturing localized frequency content of nonlinear structural seismic responses is also examined. To this end, the nonlinear dynamic response of a benchmark 20-story steel frame [28,29] to the above accelerograms is considered. It was designed by Brandow & Johnston Associates for the SAC Phase II Steel Project and is part of a typical mid- to high-rise building which meets the seismic code for the Los Angeles, California region.

The structural system consists of moment- resisting frames (MRFs), at the perimeter to engage lateral loads, and simple framing in the interior. The columns are 345 MPa steel and the floors are composite with 248 MPa steel beams and concrete. The model of the building along with information regarding various structural parameters is shown in Fig. (2). The floors are assumed to be rigid in the horizontal plane and thus diaphragmatic action holds. The inertia forces are assumed to be evenly distributed on the two moment resistant frames. Symmetry allows an in-plane 2-D analysis of half of the entire building and thus only one MRF along the weak N-S direction is considered. The mathematic model described in Ohtori et al [28] is followed for the boundary conditions and the discretization of the elastic and inertia properties of the frame. The first five natural frequencies of the frame are 0.261, 0.753, 1.30, 1.83 and 2.40 Hz. A trilinear hysteresis model for structural member bending, as the one shown in Fig. (3), is adopted. More details on the trilinear model values considered for each member can be found in Ohtori et al [28].

5. Numerical results: Adaptive Chirplet Spectrograms and Hilbert Spectra

5.1 Seismic Accelerograms

Both the MP algorithm utilizing a Gaussian chirplet dictionary, and the EMD algorithm have been employed to analyze the four accelerograms presented in Fig. (1). Adequate representations of the earthquake signals were made possible by relatively small numbers of terms: of order of fifty chirplet functions, and of less than ten intrinsic modes, in all of the cases. Further, due to the adaptive nature of the decomposition algorithms, the significant time-frequency characteristics of the earthquake signals were captured by the very first few terms. Regarding the level of sophistication of the adaptive chirplet decomposition, it is worth noting that the frequency modulation rate β_k of the chirplets h_k was found to be negligible, as it has been reported before [23]. Thus, a simpler dictionary of the three parametered Gabor atoms, instead of the four parametered Gaussian chirplets, can be used yielding practically the same signal expansion. This observation also suggests that the generation mechanisms of seismic events, the propagation of seismic waves through the geological formations and the potential influences of the surface soil layers do not produce signals whose complexity would justify the use of Gaussian chirplets as analyzing functions.

Upon expanding the accelerograms into a series of chirplet functions, the WVD is applied to yield the desired representation of these signals on the time-frequency plane. Certain plots summarizing appropriate numerical results are provided in Figs. (4), (6), (8) and (10), corresponding to the El Centro, Hachinohe, Northridge and Kobe earthquake records, respectively. In the (a) plot of each figure the standard Fourier amplitude spectrum is given. The (b) plots display the three-dimensional cross-term free adaptive

chirplet spectrograms as computed by Eq. (17). In the (c) part of the aforementioned figures contour plots of the adaptive spectrograms are presented to provide a more efficient and practically useful joint time- frequency signal representation. The mean instantaneous frequency (MIF) is superimposed, as obtained by the newly derived Eq. (19), and the time histories of the accelerograms (d) are included, as well, to facilitate the physical interpretation.

All surfaces shown in the (b) plots are exceptionally smooth throughout the time-frequency plane and manifest the capacity of the Gaussian chirplets to represent the signals considered with adequate resolution at all frequency bands of interest. By comparing the corresponding (a) and (c) plots, it is obvious that the overall frequency content provided by the Fourier amplitude spectra can equivalently be deduced by the adaptive spectrograms. However, the latter capture, additionally, the evolution of the frequencies present at every time instant of the records which illustrates the superiority of a joint time-frequency analysis over the traditional Fourier analysis for earthquake accelerograms. As expected, the higher frequencies prevail during the "growth phase" of the accelerograms and then decay following a rate that is influenced by many parameters whose consideration is beyond the scope of the present study.

In implementing the EMD, the basic algorithm and assumptions proposed by Rilling et al [12], were adopted to balance precision versus computational cost, as it has already been mentioned. The IMFs thus obtained yielded quite oscillating Hilbert spectra. Low-pass filtering of the unwrapped phase of the IMFs and their associated amplitudes by means of spline fitting was proved to be a necessity to achieve smoother results amenable to physical interpretation. In Figs. (5), (7), (9), (11), representative Hilbert

spectra (Eq. (24)) and estimates of the MIF (Eq. (25)) based on the intrinsic mode expansion are provided for the El Centro, Hachinohe, Northridge and Kobe earthquake records, respectively.

As discussed earlier, the adaptive chirplet spectrogram enjoys a solid mathematical background, which is not the case for the Hilbert spectrum based on the IMFs. Evaluation of the performance of the EMD algorithm and of the smoothing procedure of the IMFs is attempted by a qualitative comparison of the Hilbert spectra and the MIF obtained by the IMFs with the corresponding adaptive spectrograms and the MIF obtained by the Gaussian chirplets, for the four accelerograms considered. Specifically, it can be seen from the figures provided, the two different types of time-frequency spectra are consistent in the sense that the highest spectral values are attained at almost the same time intervals and frequency levels. Furthermore, the trends of the temporal change of the MIF exhibit a close similarity, even though the IMFs yield more oscillatory MIF time-histories.

5.2 Structural response

Inelastic time-history dynamic analysis was performed for the 20- story steel frame of Fig. (2) using as input the El Centro ground acceleration of Fig. (1) multiplied by various factors. The standard β-Newmark algorithm with the assumption of constant acceleration at each time step (values $\beta=1/4$, $\gamma=1/2$), was employed for the numerical integration in time. In this manner, the non linear behavior of the frame stemming from the adopted trilinear hysteresis model is properly taken into account, as described extensively in Ohtori et al [28].

The same decomposition algorithms used to analyze the seismic accelerograms were next applied to the lateral displacement response signals of the first floor of the frame under consideration as obtained by the above dynamic analysis. Herein, the objective was to assess the potential of both methods for providing valid joint time-frequency representations of non linear structural responses, for capturing the influence of nonlinearity on the evolution of the effective natural frequencies of yielding structural systems during a strong ground motion, and for demonstrating the effectiveness of the MIF for global damage detection.

In the case of the adaptive chirplet expansion it has been observed that a significantly smaller number of chirplets is required to fully describe the response signals than in the case of the seismic accelerograms. This is due to the fact that structural systems exhibit highly "resonant" transfer functions which filter the relatively broadband earthquake signal inputs yielding response signals characterized by the structural natural frequencies. Consequently, the MP algorithm readily locates the narrowband dominant components present in the structural response signals by assigning appropriate weights to the most similar analyzing functions to match efficiently these components. A Gabor atoms dictionary yields practically the same decomposition of the structural response signals as the one obtained by using Gaussian chirplets in the same way as it was noted in the case of the analysis of the earthquake records.

To demonstrate the potential of the MIF as analytical damage detection tool two extreme cases are shown in Figs. (12) and (13) where the plots included are of the same kind and order as in Fig. (10). In Fig. (12) the imposed excitation is the El Centro accelerogram reduced by a factor of 0.5 so that the frame remains in the elastic region. In

Fig. (13) the El Centro accelerogram scaled by 2.50 is used as input and the frame suffers structural damage witnessed by permanent deformation and a large offset component in the Fourier spectrum. For reference purposes the first five natural frequencies of the elastic frame are shown on the plots.

It is well known that structural systems forced to exhibit inelastic behavior are characterized by gradually reduced effective natural frequencies, due to stiffness degradation. Obviously, the variation in the "effective" natural frequencies of non linear systems is reflected on the time-dependent transfer functions they attain and thus on the output-response signals. In this context, the concentration of the energy of the response signal about the natural frequencies of the frame which decrease when the frame undergoes inelastic deformations can be readily seen in Figs. (12) and (13) in the traditional Fourier spectrum plots (a), and in the adaptive spectrograms (b), (c). Apparently, the joint time- frequency representation gives additional time localization information about the effective frequencies of the response signals and adequately captures their evolution in time.

More importantly, in this case the MIF can be interpreted as a global structural damage indicator. The fundamental theorem of linear systems states that the spectrum of the output signal is equal to the product of the Fourier transform of the input signal times the transfer function of the system. Intuitively, for any particular effective temporal segment defined such that the transfer function of the structure is assumed constant, the MIF of the response averages this product over the frequency domain. Note that during the first 25 seconds of both of the response signals examined in Figures (12c) and (13c) the MIF oscillates about, roughly, the same mean value. It is clear that in this case the

MIF averages the product of the effective transfer function of the structure with the spectrum of the excitation. Subsequently, the 30^{th} second approximately marks the effective duration of this particular input; practically the rest of the output signals correspond to free vibration responses. As expected, after this time instant, the MIF significantly decreases and remains in much lower levels for the scaled by 2.50 El Centro input where the frame undergoes plastic deformations. However, in the elastic case, it converges to a value similar to that attained at the beginning of the seismic event, since the dynamic characteristics of the structure remain the same.

Prior to the application of the EMD, the response signals considered in this analysis were limited to a bandwidth of approximately 0-5 Hz. The same algorithm was applied as before and yielded again eight to ten IMFs for signal durations of 60 sec sampled at the Nyquist frequency. Apparently, the number of the IMFs and the computational cost of the EMD algorithm depend primarily on the length of the data and not on the frequency content of the data which was the case for the MP algorithm and adaptive chirplet decomposition, as was reported above.

In Figs. (14) and (15), the Hilbert spectra of the decomposed lateral displacement response of the first floor for the El Centro accelerogram input scaled by 0.50 and 2.50 are shown, respectively. The natural frequencies of the linear elastic system and the MIF are also superimposed. The results show that the obtained IMFs are capable of capturing the evolution of the natural frequencies of the structural system under consideration. Nevertheless, the Hilbert spectra and the temporal variation of the MIF are not as smooth, and amenable to physical interpretation compared to the corresponding adaptive spectrograms of the chirplet analysis. There is an apparent mode mixing in the sense that

some IMFs are “attracted” by different natural frequencies during various time intervals. This phenomenon can be reduced by introducing restrictions on the time interval between successive extreme points attained by the IMFs based on the natural frequencies of the analyzed system. Furthermore, additional low-pass filtering of the unwrapped phase and amplitude of the IMFs can be used to yield less oscillating Hilbert spectra, at the expense of poorer resolution. However, the later improvements require increased user/analyst interaction in the form of parameter adjustments, rendering often the method less appealing for practical purposes [27].

6. Concluding remarks

The present article has focused on the appropriateness, level of sophistication, and comparative efficiency of certain adaptive signal analysis techniques for time-frequency representation of non-stationary signals encountered in earthquake engineering problems. In this regard, the adaptive chirplet transform (incorporating the MP algorithm), and the EMD have been employed to analyze historic earthquake accelerograms and inelastic structural response time histories to seismic signal inputs. Signals of this nature are inherently non stationary as their intensity and frequency content varies with time and thus require a joint time- frequency representation.

In this context, four ground acceleration records pertaining to two near-field and two far- field major earthquake events have been decomposed into chirplet functions and IMFs, and the WVD and Hilbert spectra of the decomposed signals have been obtained respectively. A relatively small number of analyzing functions has been found to be sufficient for the adequate approximation of the signals, while their main patterns and energy content have been captured by the very few first terms. In addition, it has been

found that a much simpler dictionary comprising Gabor atoms instead of Gaussian chirplets yields an almost identical unfolding of the seismic signals in the time-frequency domain and thus can be adopted to reduce the computational cost. The appropriateness of the time-frequency representation to capture the evolving frequency content in time, unlike the traditional Fourier amplitude spectrum, has been pointed out. Indeed, both representations can be used as stand-alone time-frequency analysis tools. Note however that despite the qualitative similarity of the two mathematically different representations, the WVD is smoother and lends itself to easier physical interpretation compared to the Hilbert spectrum.

Furthermore, both adaptive methods have been applied to the lateral displacement response of the first floor of a 20-story steel frame exposed to one of the four accelerograms scaled by appropriate factors to simulate undamaged and severely damaged conditions for the structure. It has been found that significantly less chirplet functions were sufficient to fully describe the response signals, than in the case of the strong ground motion accelerograms, while the number of the required IMFs remained practically the same, suggesting that the adaptive chirplet transform is much more economical in terms of computational time. This observation can be attributed to the highly resonant filtering effect of structural systems to broadband strong ground excitations which facilitates the approximation of the response via chirp- type functions. Furthermore, this concentration of the frequency content of the response signals about the natural frequencies of the structure caused a characteristic mode-mixing in the IMFs which obscures the physical interpretation of the Hilbert spectrum. This difficulty can be moderated by imposing appropriate restrictions when identifying the extreme points

during the EMD of the signal and by further smoothing the unwrapped phase and amplitude of the resulting IMFs. Clearly, these measures require increased user/analyst interaction in the form of parameter adjustments, and may render the adaptive chirplet decomposition more attractive in practice vis-à-vis the EMD.

The potential of time-frequency representations of structural response signals as a detection tool for global structural damage has been also pointed out. Specifically, attention has been focused on the temporal evolution of the mean instantaneous frequency. Indeed, if the structure is forced to exhibit inelastic behavior, the mean instantaneous frequency reduces significantly reflecting the overall decrease of the effective frequencies which is due to the structural stiffness degradation.

In conclusion, the findings of the present study show that both the adaptive chirplet decomposition and the intrinsic modes decomposition are viable options for joint time-frequency analyses of seismic signals. Furthermore, considering collectively these two decompositions and the competing wavelet based decomposition, it is perhaps premature to dispute any of the three as clearly the most advantageous for earthquake engineering applications.

7. Acknowledgements

The financial support of this work by a grant from NSF is greatly acknowledged.

References

1. Cohen L. Time- Frequency Analysis. Upper Saddle River, NJ: Prentice-hall; 1995.

2. Burrus CS, Gopinath RA, Guo H. Introduction to wavelets and wavelet transforms- A primer. Upper Saddle River, NJ: Prentice-hall; 1997.

3. Mallat S. A wavelet tour of signal processing. London: Academic Press; 1998.

4. Mann S, Haykin S. The chirplet transform: Physical considerations. IEEE Trans Signal Process 1995;43(11):2745-2761.

5. Baraniuk RG, Jones DL. Wigner- based formulation of the chirplet transform. IEEE Trans Signal Process 1996;44(12):3129-3135.

6. Huang NE, Shen Z, Long SR, Wu MC, Shih HH, Zheng Q, Yen NC, Tung CC, Liu HH. The empirical mode decomposition and the Hilbert spectrum for nonlinear and non-stationary time series analysis. Proc R Soc Lond A 1998;454:903-995.

7. Qian S. Introduction to time-frequency and wavelet transforms. Upper Saddle River, NJ: Prentice-hall; 2001.

8. Chen SS, Donoho DL, Saunders MA. Atomic decomposition by basis pursuit. SIAM J. Sci Comput 1998;20(1):33-61.

9. Mallat S, Zhang Z. Matching pursuits with time-frequency dictionaries. IEEE Trans Signal Process 1993;41(12):3397-3415.

10. Qian S, Chen D. Signal representation via adaptive normalized Gaussian functions. Signal Process 1994;36(1):1-11.

11. Yin Q, Qian S, Feng A. A fast refinement for adaptive gaussian chirplet decomposition. IEEE Trans Signal Process 2002;50(6):1298-1306.

12. Rilling G, Flandrin P, Goncalves P. On empirical mode decomposition and its algorithms. In: IEEE-EURASIP Workshop on nonlinear signal and image processing. NSIP-03, GRADO(I); 2003.

13. Gabor D. Theory of communication. J. IEEE 1946;93(3):429-457.

14. Spanos PD, Failla G. Wavelets: Theoretical concepts and vibrations related applications. Shock Vib Digest 2005;37(5):359-375.

15. Boashash B. Estimating and interpreting the instantaneous frequency of a signal. I. Fundamentals. Proc IEEE 1992;80(4):520-538.

16. Flandrin P, Goncalves P. Empirical mode decompositions as data-driven wavelet-like expansions. International Journal of Wavelets, Multiresolution & Information Processing, 2004;2(4):477-496.

17. Wang J, Fan L, Qian S, Zhou J. Simulations of non-stationary frequency content and its importance to seismic assessment of structures. Earthquake Eng Struct Dyn 2002;31:993-1005.

18. Huang NE, Chern CC, Huang K, Salvino LW, Long SR, Fan KL. A new spectral representation of earthquake data: Hilbert spectral analysis of station TCU129, Chi-Chi, Taiwan, 21 September 1999. Bull Seism Soc Amer 2001;91(5):1310-1338.

19. Loh CH, Wu TC, Huang NE. Application of the empirical mode decomposition-Hilbert spectrum method to identify near-fault ground-motion characteristics and structural responses. Bull Seism Soc Amer 2001;91(5):1339-1357.

20. Zhang RR, Ma S, Hartzell S. Signatures of the seismic source in EMD-based characterization of the 1994 Northridge, California, earthquake recordings. Bull Seism Soc Amer 2003;93(1):501-518.

21. Zhang RR, Ma S, Safak E, Hartzell S. Hilbert-Huang transform analysis of dynamic and earthquake motion recordings. J. Eng Mech ASCE 2003;129(8):861-875.

22. Yang JN, Lei Y, Lin S, Huang N. Hilbert-Huang based approach for structural damage detection. J. Eng Mech ASCE 2004;130(1):85-95.

23. Yan B, Miyamoto A. A comparative study of modal Parameter identification based on wavelet and Hilbert-Huang transforms. Computer- aided civil and infrastructure engineering. 2006;21(1):9-23.

24. Xu YL, Chen J. Structural damage detection using empirical mode decomposition: Experimental investigation. J. Eng Mech ASCE 2004;130(11):1279-1288.

25. Zhang RR, Denmark LV, Liang J, Hu Y. On estimating site damping with soil non-linearity from earthquake records. Int. J. Non-linear Mech. 2004;39:1501-1517.

26. Huang NE, Attoh-Okine NO, editors. The Hilbert-Huang transform in engineering. Boca Raton, FL: CRC Press; 2005.

27. Kijewski-Correa T, Kareem A. Efficacy of Hilbert and wavelet transforms for time-frequency analysis. J. Eng Mech ASCE 2006;132(10):1037-1049.

28. Ohtori Y, Christenson RE, Spencer BFJ, Dyke SJ. Benchmark structural control problems for seismically excited nonlinear buildings. J. Eng Mech ASCE 2004;130(4):366-385.

29. Spencer BFJ, Christenson RE, Dyke SJ. Next generation benchmark control problems for seismically excited buildings. In: Proceedings of the 2nd World Conference on Structural Control. Kobori T et al. editors. Vol.2:1135–1360. Wiley, New York, 1999.

30. Roesset JM. Nonlinear dynamic response of frames. In: 8th Symposium on Earthquake Engineering. Roorkee, 1986;1:435-442.

31. Boashash B. Estimating and interpreting the instantaneous frequency of a signal. II. Algorithms and applications. Proc IEEE 1992;80(4):540-568.

32. Olhede S, Walden AT. The Hilbert spectrum via wavelet projections. Proc R Soc Lond A. 2004;460(2044):955-975.

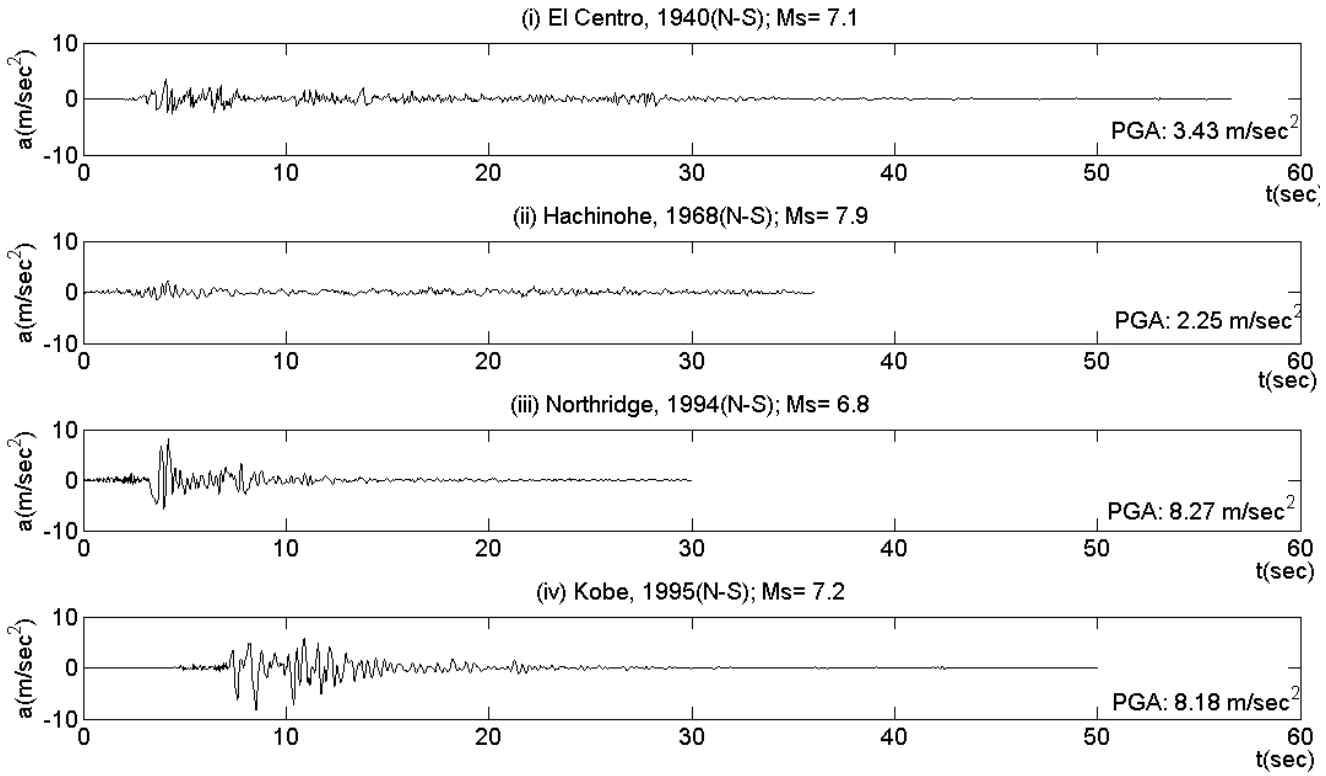

Figure (1): Earthquake accelerograms considered

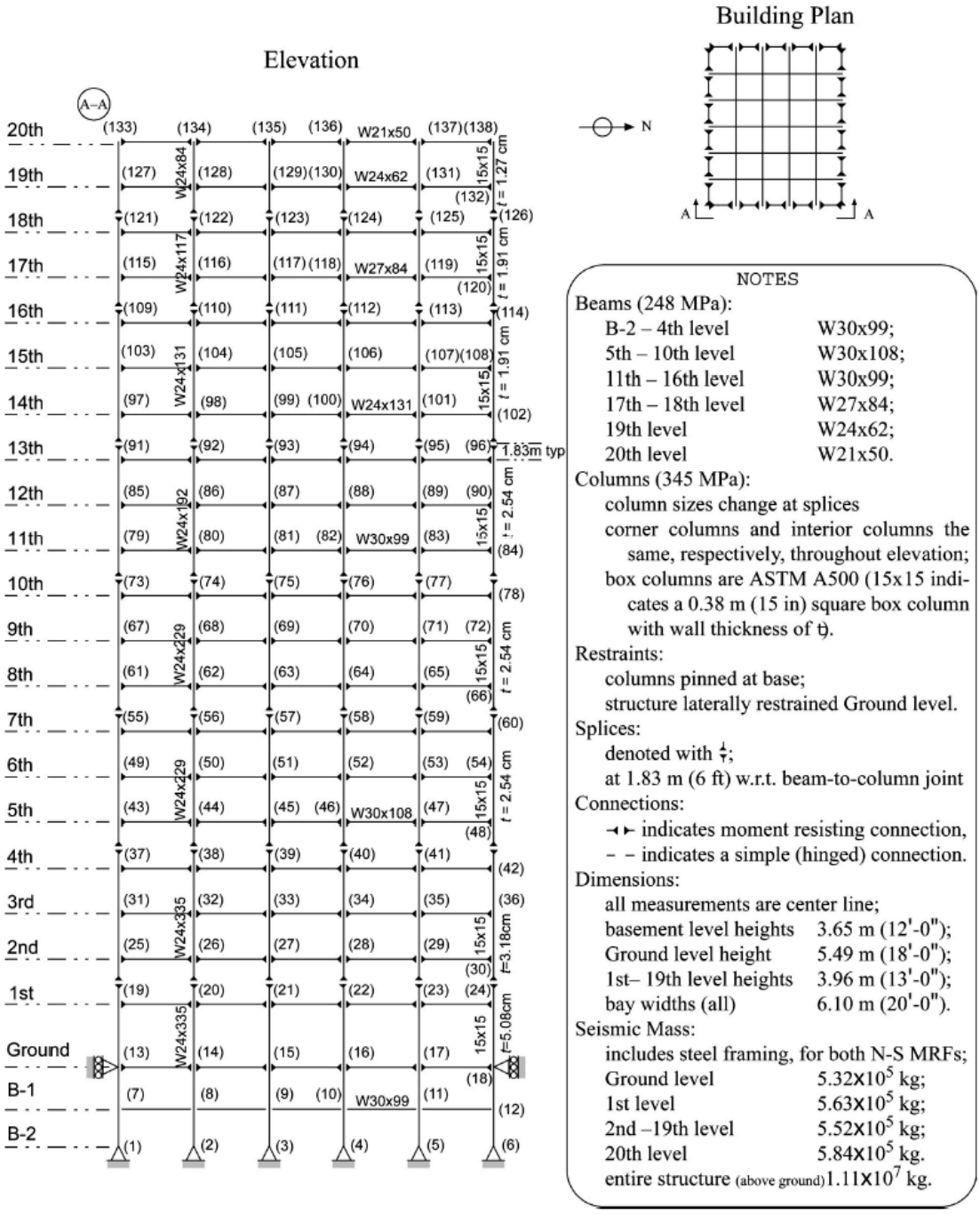

Figure (2): Benchmark 20-story steel frame used in the analysis of typical mid- to high-rise building's response to earthquake excitations (after Spencer et al. [29])

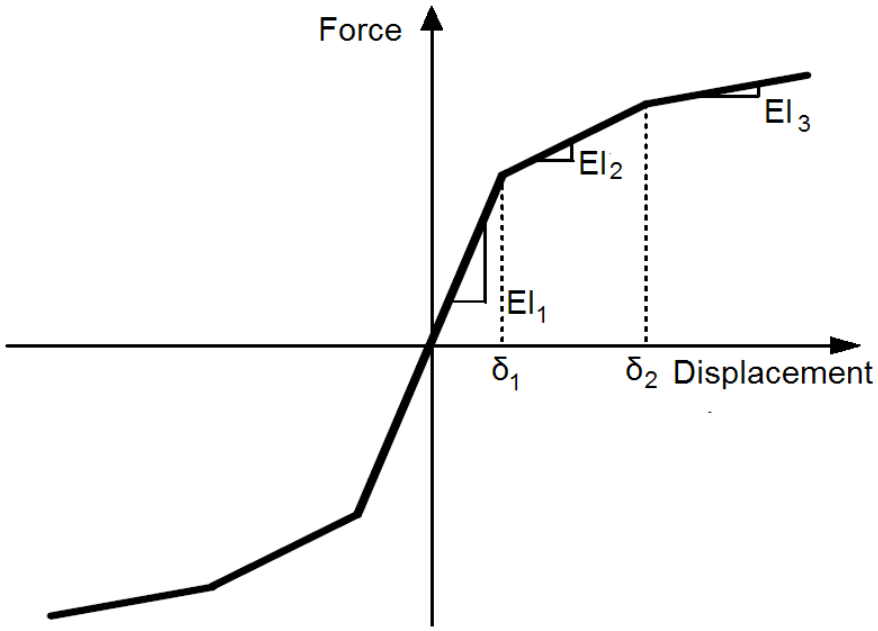

Figure (3): Trilinear hysteresis model for structural member bending

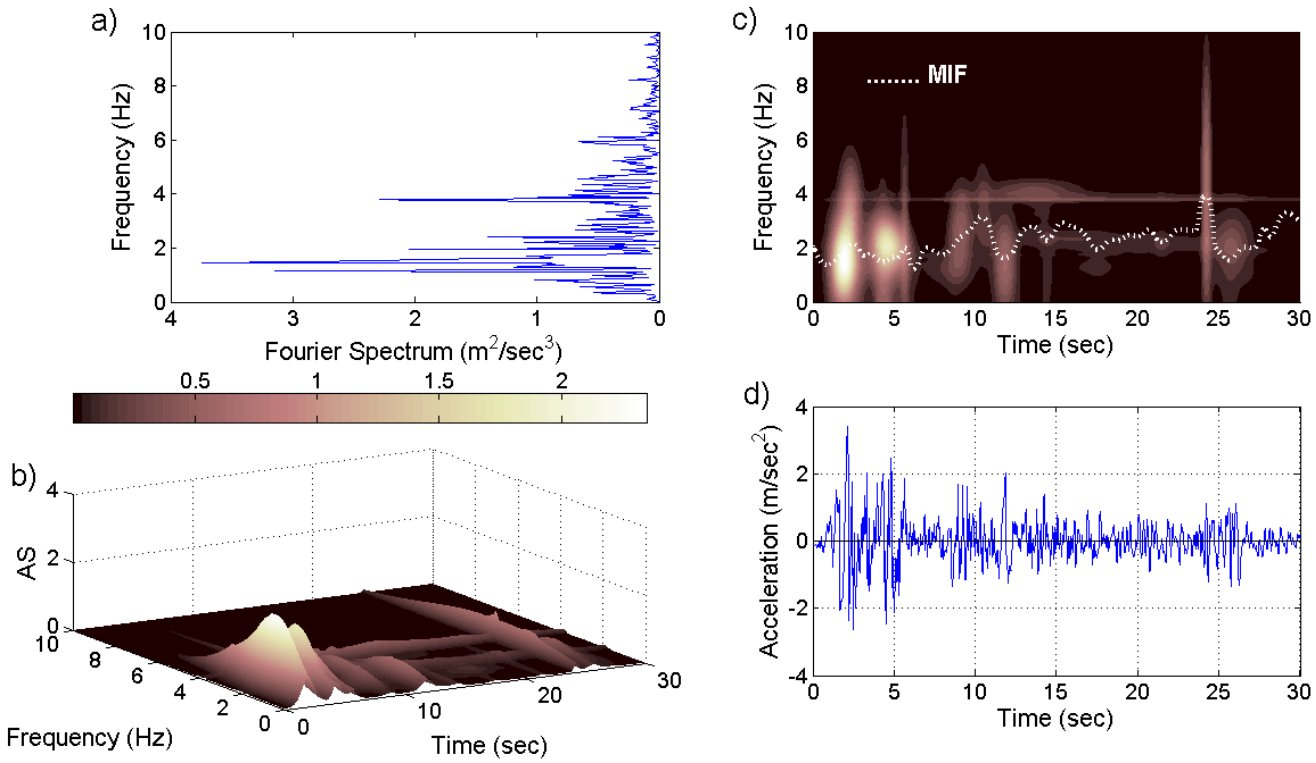

Figure (4): Joint time-frequency analysis of the El Centro accelerogram record via adaptive Gaussian chirplet expansion in conjunction with the Wigner-Ville distribution

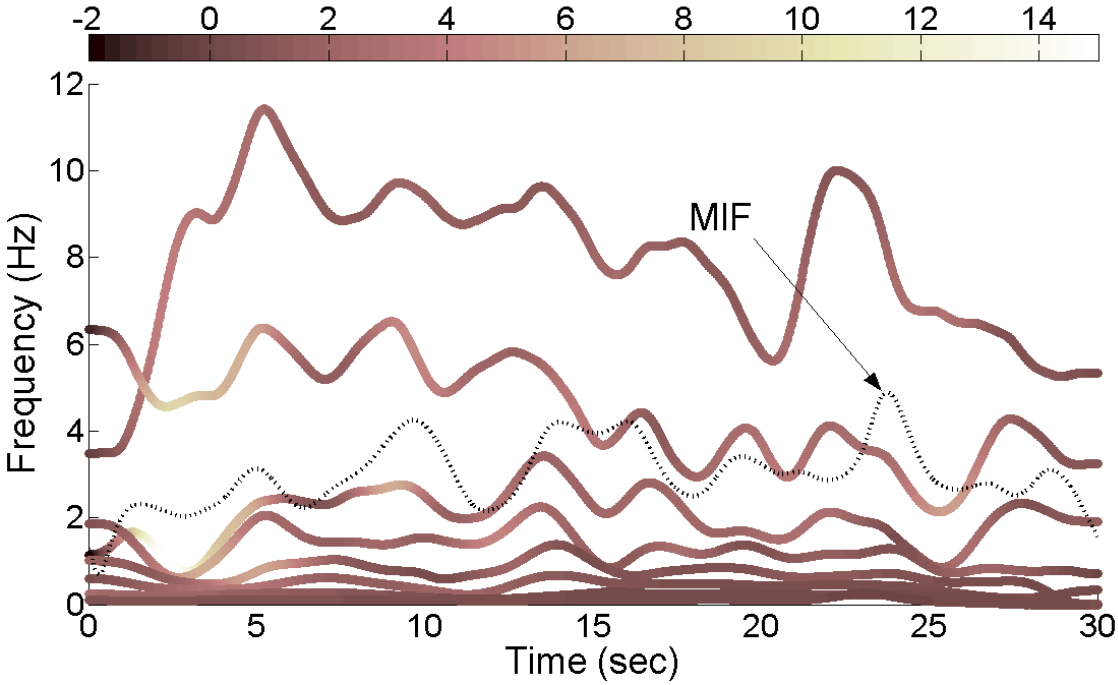

Figure (5): Hilbert spectrum and mean instantaneous frequency of the El Centro accelerogram record via Intrinsic Mode Functions

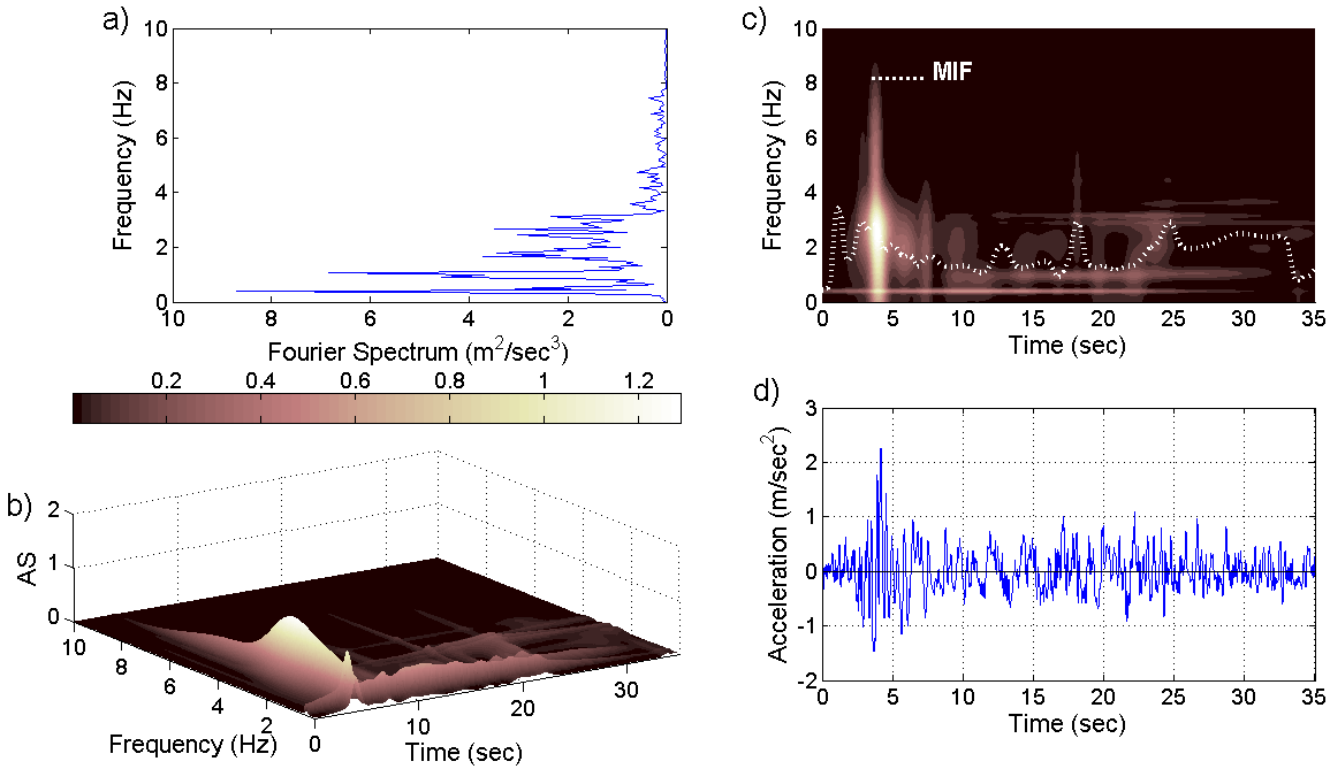

Figure (6): Joint time-frequency analysis of the Hachinohe accelerogram record via adaptive Gaussian chirplet expansion in conjunction with the Wigner-Ville distribution

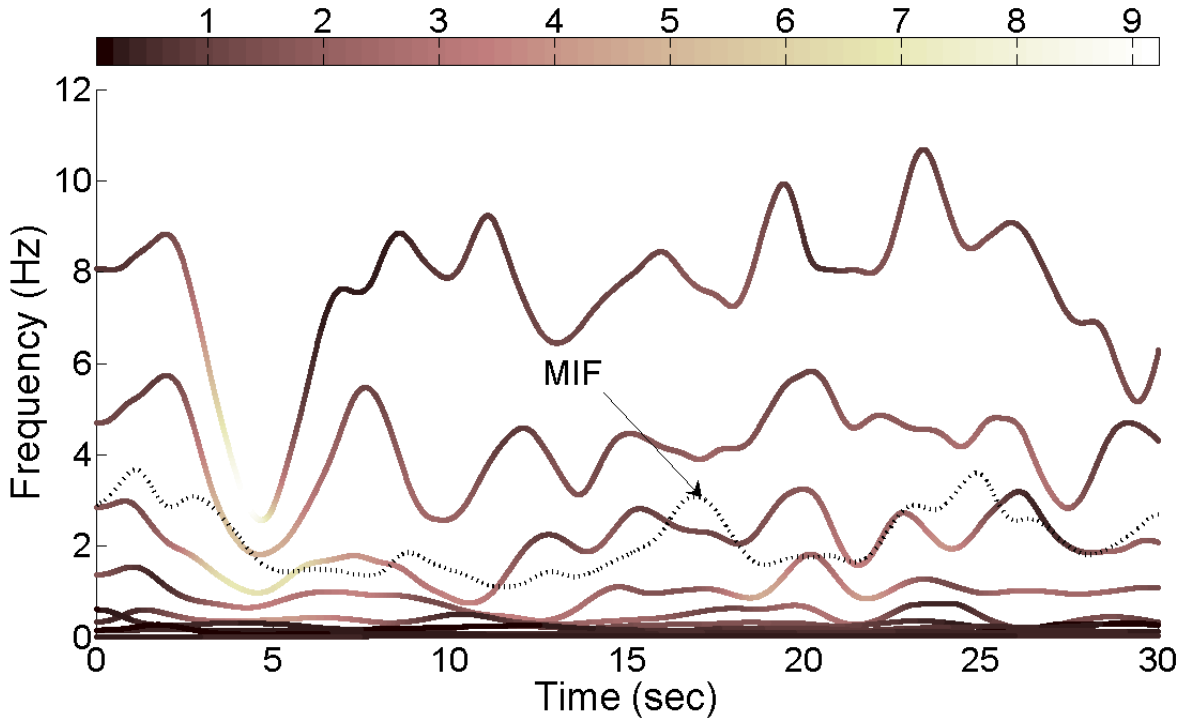

Figure (7): Hilbert spectrum and mean instantaneous frequency of the Hachinohe accelerogram record via Intrinsic Mode Functions

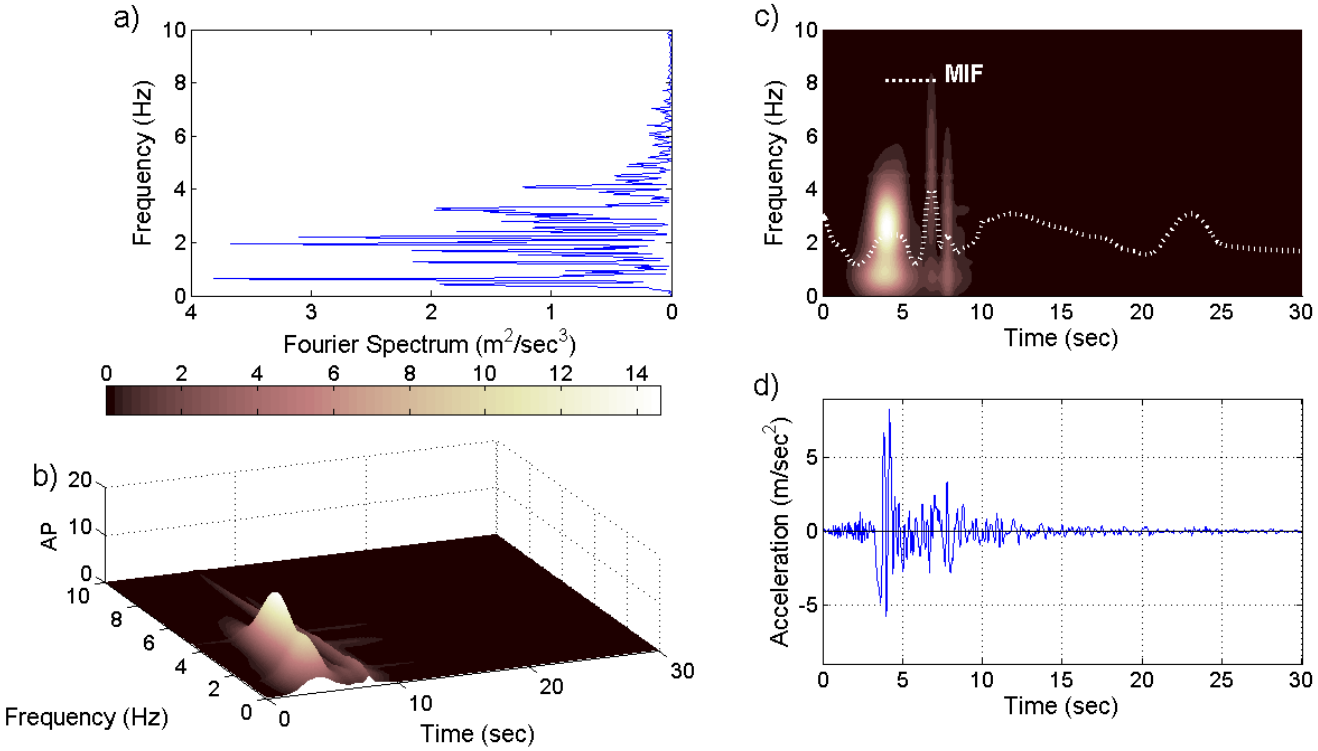

Figure (8): Joint time-frequency analysis of the Northridge accelerogram record via adaptive Gaussian chirplet expansion in conjunction with the Wigner-Ville distribution

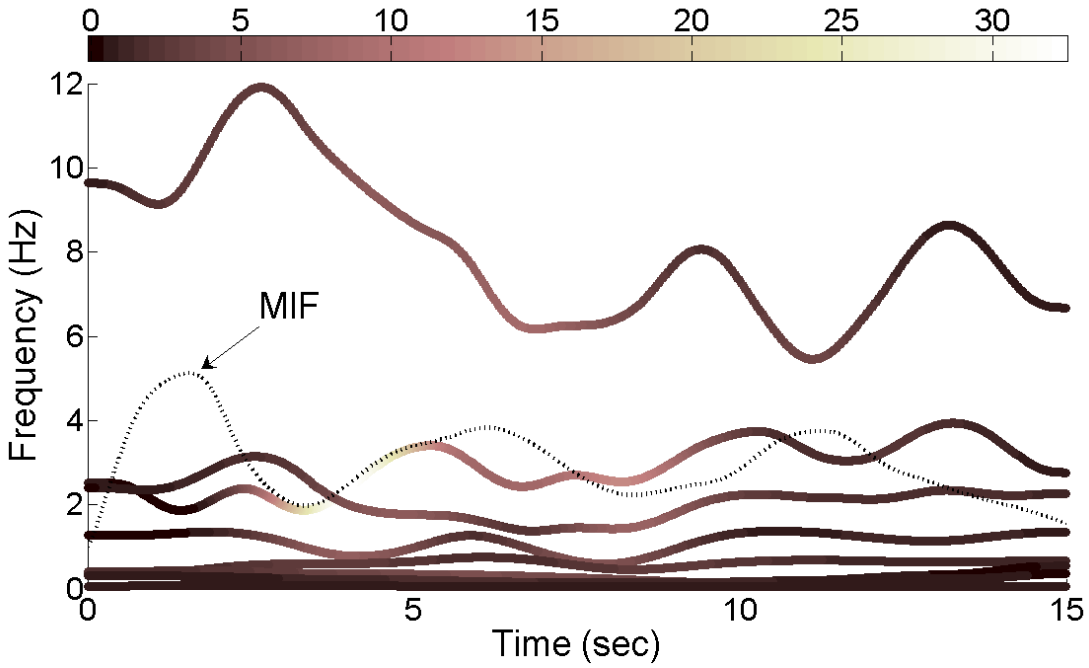

Figure (9): Hilbert spectrum and mean instantaneous frequency of the Northridge accelerogram record via Intrinsic Mode Functions

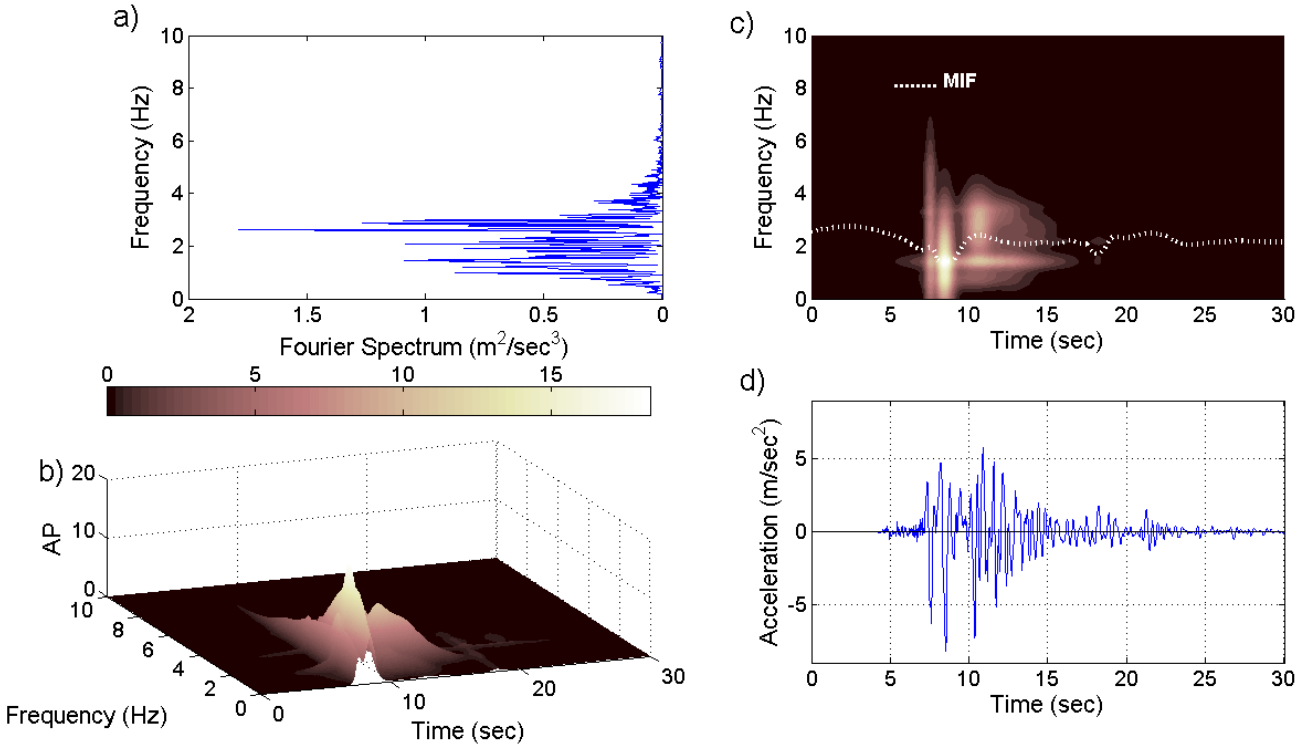

Figure (10): Joint time-frequency analysis of the Kobe N-S accelerogram record via adaptive Gaussian chirplet expansion in conjunction with the Wigner-Ville distribution

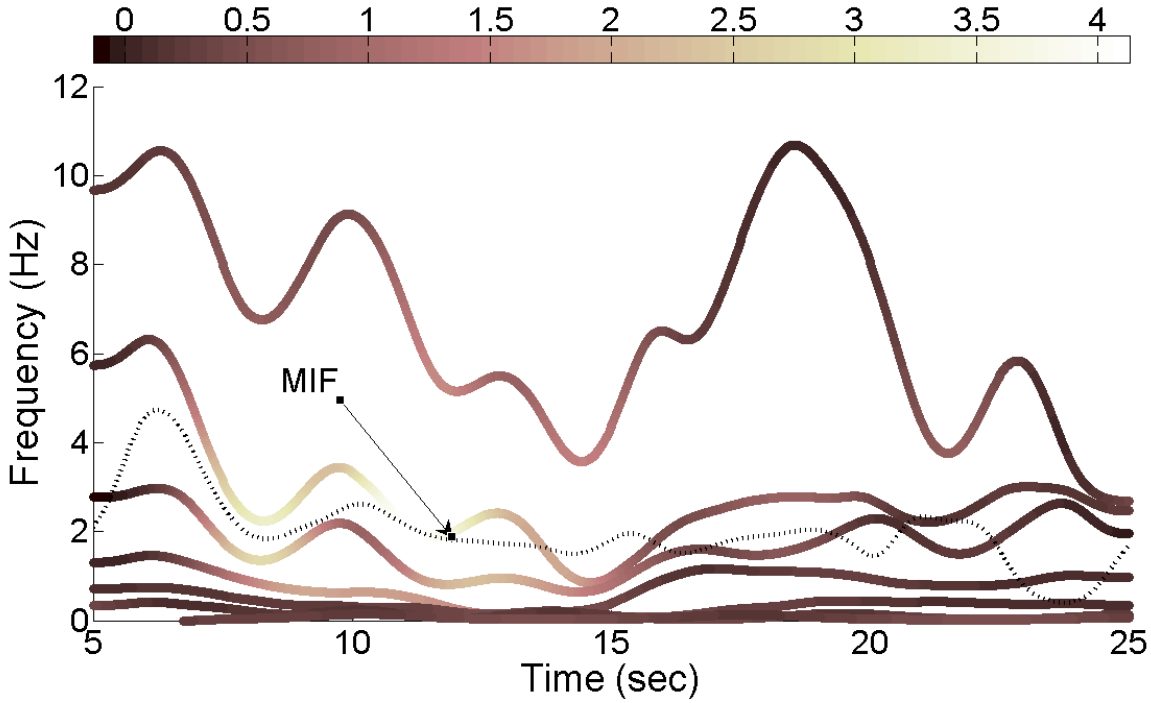

Figure (11): Hilbert spectrum and mean instantaneous frequency of the Kobe accelerogram record via Intrinsic Mode Functions

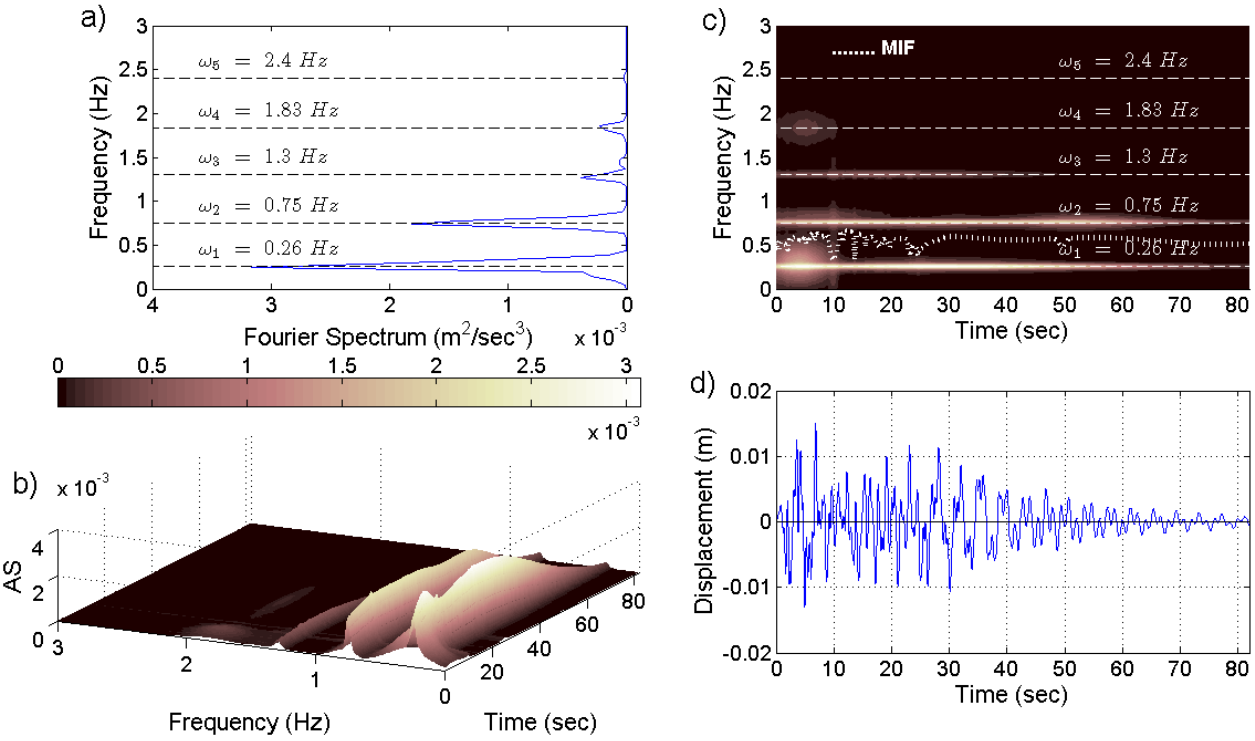

Figure (12): Adaptive chirplet spectrogram of the first floor lateral displacement response to 0.50· El Centro ground acceleration input

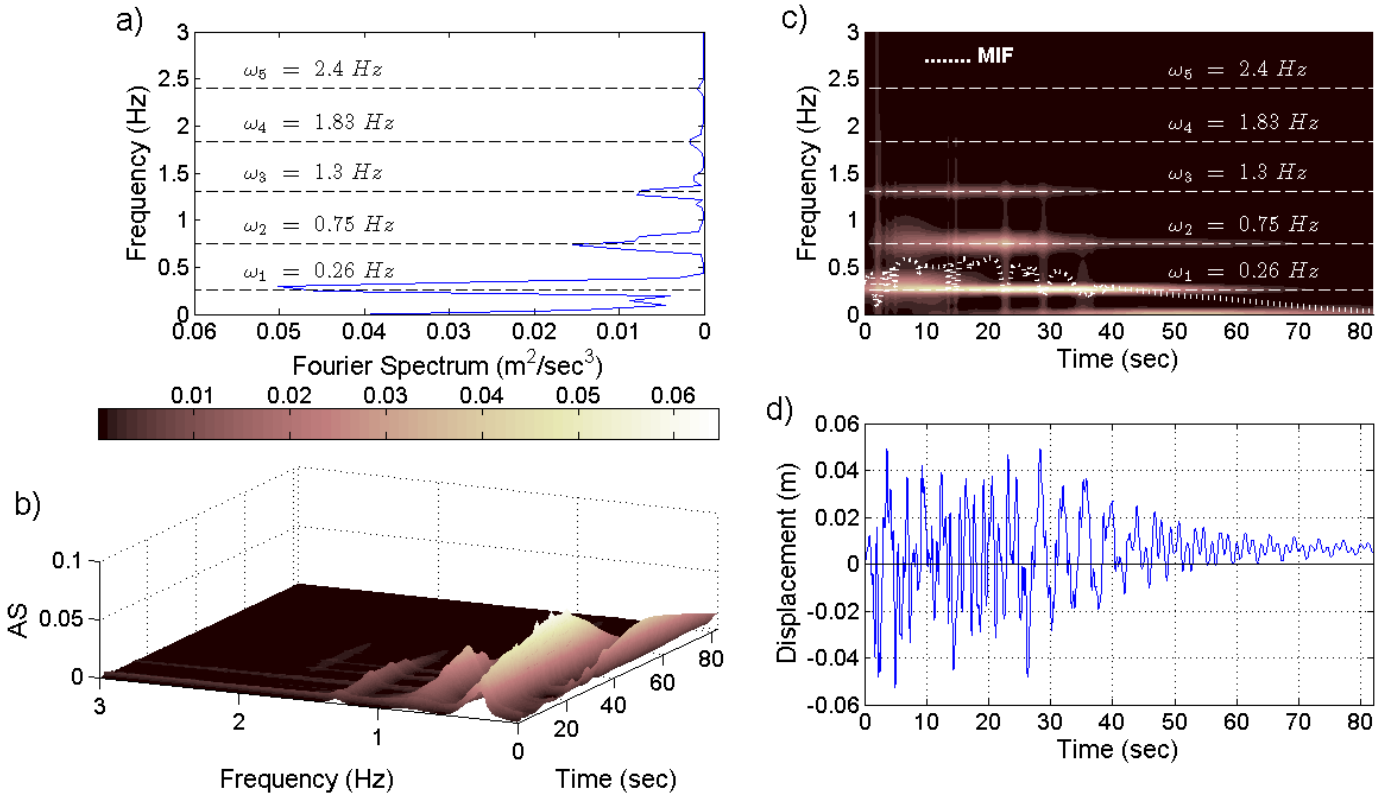

Figure (13): Adaptive chirplet spectrogram of the first floor lateral displacement response to 2.50· El Centro ground acceleration input

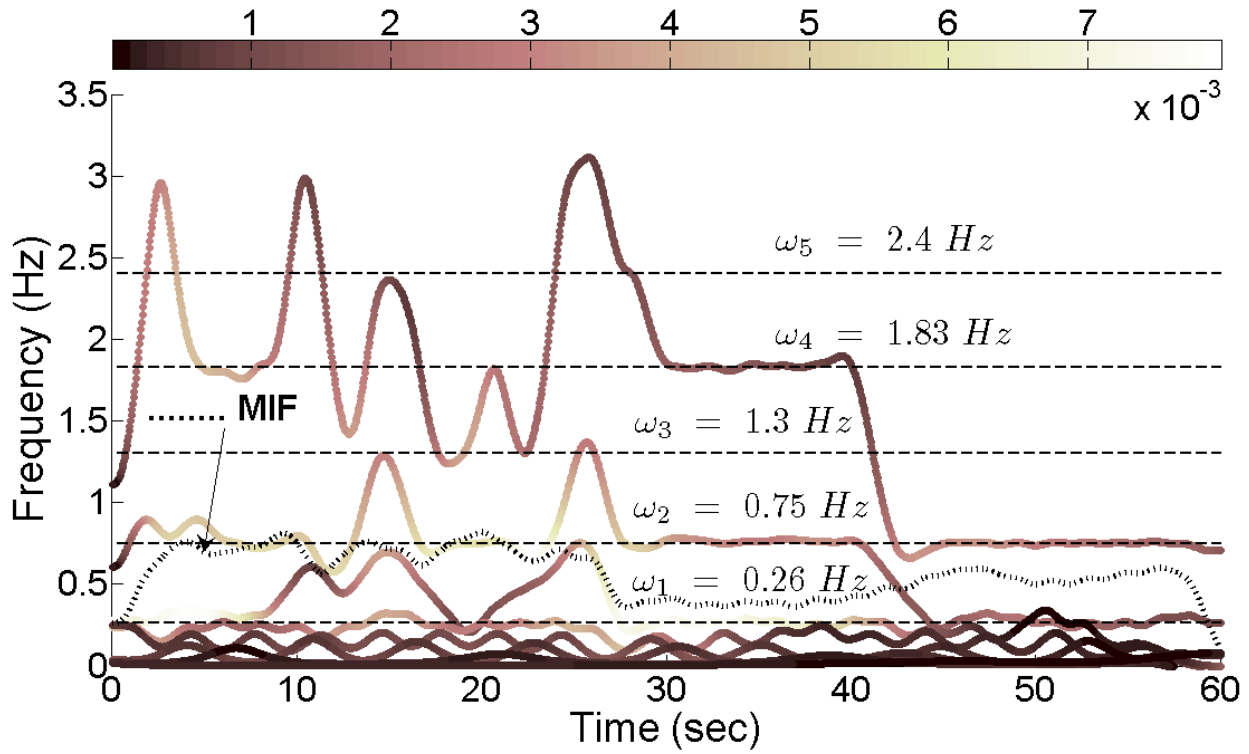

Figure (14): Hilbert spectra via Intrinsic Mode Functions of the first floor lateral displacement response to 0.50· El Centro ground acceleration input

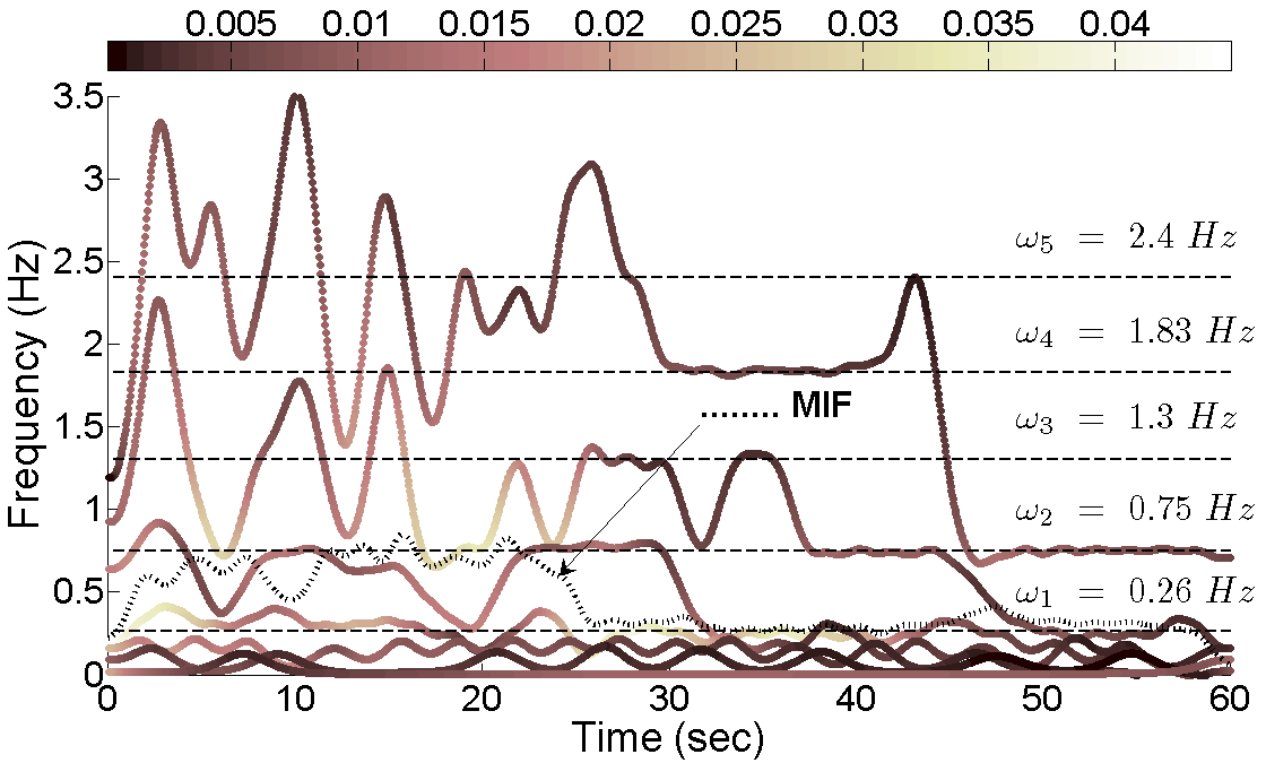

Figure (15): Hilbert spectra via Intrinsic Mode Functions of the first floor lateral displacement response to 2.50· El Centro ground acceleration input